Structure of Carbamoyl Phosphate Synthetase: A Journey of 96 Å from Substrate to Product[†,‡]

James B. Thoden,[§] Hazel M. Holden,*[,§] Gary Wesenberg,[§] Frank M. Raushel,[||] and Ivan Rayment*[,§]

Institute for Enzyme Research, Graduate School, and Department of Biochemistry, College of Agriculture, University of Wisconsin, Madison, Wisconsin 53705, and Department of Chemistry, Texas A&M University, College Station, Texas 77843

Received March 4, 1997; Revised Manuscript Received March 25, 1997[⊗]

ABSTRACT: Carbamoyl phosphate synthetase catalyzes the production of carbamoyl phosphate from bicarbonate, glutamine, and two molecules of MgATP. As isolated from *Escherichia coli*, the enzyme has a total molecular weight of ∼160K and consists of two polypeptide chains referred to as the large and small subunits. Here we describe the X-ray crystal structure of this enzyme determined to 2.8 Å resolution in the presence of ADP, Mn^{2+}, phosphate, and ornithine. The small subunit is distinctly bilobal with the active site residues located in the interface formed by the NH_2- and COOH-terminal domains. Interestingly, the structure of the COOH-terminal half is similar to that observed in the trp*G*-type amidotransferase family. The large subunit can be envisioned as two halves referred to as the carboxyphosphate and carbamoyl phosphate synthetic components. Each component contains four distinct domains. Strikingly, the two halves of the large subunit are related by a nearly exact 2-fold rotational axis, thus suggesting that this polypeptide chain evolved from a homodimeric precursor. The molecular motifs of the first three domains observed in each synthetic component are similar to those observed in biotin carboxylase. A linear distance of ∼80 Å separates the binding sites for the hydrolysis of glutamine in the small subunit and the ATP-dependent phosphorylations of bicarbonate and carbamate in the large subunit. The reactive and unstable enzyme intermediates must therefore be sequentially channeled from one active site to the next through the interior of the protein.

Carbamoyl phosphate synthetase (CPS) catalyzes one of the most remarkable reactions ever described in biological chemistry. This enzyme assembles carbamoyl phosphate from bicarbonate, glutamine, and two molecules of MgATP coupled with the production of glutamate, phosphate, and two molecules of MgADP. On the basis of isotopic labeling studies and the discovery of three additional partial reactions, Anderson and Meister (*1*) postulated that carbamoyl phosphate is constructed within the active site(s) of this enzyme by a series of four separate chemical reactions as illustrated below:

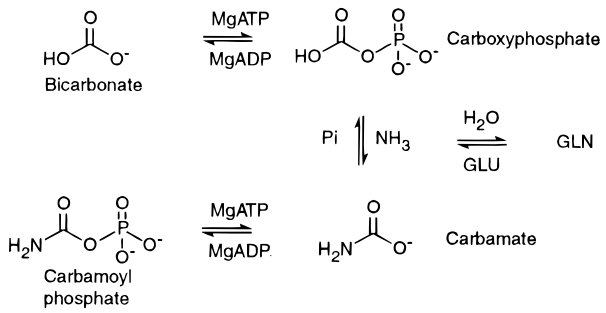

There are thus a minimum of three discrete, highly reactive, and unstable intermediates in this reaction scheme: carboxyphosphate, carbamate, and ammonia. The existence of these intermediates and the order of events have been supported by steady state and rapid mixing kinetic analyses (*2, 3*).

The synthesis of carbamoyl phosphate is critical for the initiation of two separate biosynthetic pathways. In one, carbamoyl phosphate is coupled to aspartate in a reaction catalyzed by aspartate transcarbamoylase. The carbon and nitrogen nuclei of carbamoyl phosphate are ultimately incorporated in the aromatic moieties of pyrimidine nucleotides such as UMP. In the second pathway, carbamoyl phosphate is condensed with ornithine at the start of the urea cycle and is utilized for the detoxification of ammonia and the biosynthesis of arginine. As would be anticipated, CPS therefore displays a complex pattern of metabolic regulation. The precise set of allosteric ligands depends on the particular biological and physiological niche of the cell where CPS resides. With the CPS from *Escherichia coli*, where there is a single enzyme for both pathways, the protein is allosterically activated by ornithine and inhibited by UMP. The mode of inhibition is primarily, but not exclusively, through modulation of the Michaelis constant for MgATP by 1 order of magnitude in either direction (*4, 5*). In contrast, the human liver enzyme utilized for the urea cycle requires *N*-acetyl glutamate as an allosteric activator (*6*).

The protein, as isolated from *E. coli*, is a heterodimer. The smaller subunit with a molecular weight of 42K functions as the site of glutamine hydrolysis and as a device for the delivery of ammonia to the larger subunit (*7*). This larger subunit, with a molecular weight of 118K, is known to catalyze the synthesis of carbamoyl phosphate with only ammonia as the nitrogen source (*8*). It also serves as the site of binding for the allosteric ligands, and the divalent

[†] Supported in part by NIH Grants DK47814 (H.M.H.), DK30343 (F.M.R.), and AR35186 (I.R.) and the Robert A. Welch Foundation (A-840) (F.M.R.).

[‡] Coordinates have been deposited in the Brookhaven Protein Data Bank (1JDB).

* To whom correspondence should be addressed. E-mail: Ivan@enzyme.wisc.edu or Holden@enzyme.wisc.edu. Phone: (608) 262-0529 (I.R.) and (608) 262-4988 (H.M.H.). Fax: (608) 265-2904.

[§] University of Wisconsin.

[||] Texas A&M University.

[⊗] Abstract published in *Advance ACS Abstracts,* May 1, 1997.

S0006-2960(97)00503-5 CCC: $14.00

and monovalent cations. Sequencing of the car*AB* genes from *E. coli* by Lusty and co-workers has revealed two quite interesting features (*9, 10*). Significant portions of the small subunit are homologous to the trp*G*-type amidotransferases, of which GMP synthetase is a good example (*10*). This class of amidotransferases utilizes an active site cysteine (identified in CPS as Cys^{269}) to initiate a nucleophilic attack on the carboxamide group of glutamine (*11*). More surprisingly, the large subunit has been shown to display a homologous repeat sequence where residues $Met^{1}-Arg^{400}$ are 40% identical with residues $Ala^{553}-Leu^{933}$ (*9*). Each of these two putative physical components has been shown to contain one of the two MgATP binding sites required for the synthesis of carbamoyl phosphate (*12*). Accordingly, the N-terminal half of the large subunit catalyzes the production of carboxyphosphate while the second half facilitates the phosphorylation of carbamate (*12*−*15*). Indeed, Lusty has postulated that the present day enzyme arose by a gene duplication event from a more primitive enzyme containing kinase activity (*9*).

In this report, we describe the three-dimensional X-ray crystal structure of CPS isolated from *E. coli*. This endeavor was initiated to answer a number of fundamental questions concerning the molecular architecture and mechanistic features of a protein with such enormous complexity. How, for example, does the enzyme orchestrate the synthesis and stabilization of three separate reaction intermediates? Are the three (or four) active sites spatially distinct, or does the bicarbonate situate itself in the center of a single active site where it can then be sequentially phosphorylated, amidated, and finally rephosphorylated without moving? If the active sites are separated by a significant distance, can one deduce any mechanistic information concerning the forces involved in diffusional channeling without the uncoupling of the separate chemical reactions? How similar are the two putative synthetase domains, and what are the functions for those amino acid residues conserved in one domain and not in the other? Finally, how are the conformational changes induced by the binding of ornithine and UMP to the enzyme transmitted to the active site utilized for the phosphorylation of carbamate?

MATERIALS AND METHODS

Protein used in this investigation was purified as described (*16*) and crystallized at 4 °C from 8% PEG 8000, 0.65 M tetraethylammonium chloride, 100 mM KCl, 2.5 mM ADP, 0.5 mM $MnCl_2$, 0.5 mM ornithine, and 15 mM HEPES/HEPPS at pH 7.4 with a protein concentration of 3−4 mg/mL. Diamond-shaped crystals appeared after 2 weeks to 2 months (*17*) and achieved maximum dimensions of 2.5 × 1.0 × 1.0 mm after 4−6 months.

The structure was determined by multiple isomorphous replacement (mir) from crystals belonging to the space group $P2_12_12_1$ with unit cell dimensions of $a = 154.1$ Å, $b = 166.4$ Å, and $c = 338.4$ Å. The asymmetric unit contained a tetramer with a total molecular weight of 637 016 Da, thereby presenting a challenging X-ray crystallographic problem. The key to solving the structure of CPS was in the accurate and reproducible X-ray data collection strategy employed. Initially, it was believed that the best approach for determining the three-dimensional structure of such a large protein would be to rapidly cool the crystals and utilize synchrotron radiation for X-ray data collection since the crystals were exceedingly fragile. Indeed, the crystals could be flash-cooled, and in this state, they diffracted to a nominal resolution of 2.0 Å. Unfortunately, it proved difficult to attain this cryogenic state in a reproducible manner as X-ray data from individual native crystals, presumably treated in identical manners, scaled together with an R_{merge} of >20%. This systematic error precluded any meaningful interpretation of the Patterson functions calculated from putative heavy atom derivatives. It was found, however, that X-ray data sets collected from crystals cooled to −15 °C using a multiwire area detector were highly reproducible to 5 Å resolution (Table 1).

Prior to X-ray data collection, the crystals were stabilized by transferring them to a synthetic mother liquor containing 1 M tetraethylammonium chloride, 8% PEG 8000, 200 mM KCl, 2 mM $MnCl_2$, 2 mM ornithine, and 5 mM ADP buffered at pH 7.4 with 15 mM HEPES/HEPPS. X-ray data were recorded at −15 °C with CuKα radiation from a Rigaku RU200 X-ray generator operated at 50 kV and 90 mA and equipped with a 300 μm focal cup and Göbel focusing optics on a Siemens HiStar area detector. A helium path was utilized to reduce air absorption. The X-ray data were collected at a crystal-to-detector distance of 300 mm in frames with a 0.15° angular width, processed with XDS (*18, 19*), and internally scaled with XCALIBRE (*20*). Native X-ray data to 2.8 Å resolution were recorded from nine crystals to yield 698 495 measurements which reduced to 206 423 unique reflections with an R_{merge} of 7.4%. The native X-ray set was 96.6% complete to 2.8 Å resolution.

More than 50 heavy atom compounds were surveyed as potential derivatives. This screen was performed by collecting an X-ray data set to 4.8 Å resolution from a single crystal for a given compound and concentration. The isomorphous differences between the derivative and native data set were examined as a function of resolution to determine if the changes were uniform. Many compounds that showed significant overall differences exhibited only small changes at low resolution, thereby indicating a lack of isomorphism. Promising candidates were collected in duplicate to test for reproducibility. From this search, a total of four heavy atom derivatives was found that were utilized in this structural investigation, each of which contained 12−32 heavy atom binding sites.

Difference Patterson maps calculated from the promising derivatives at the concentrations of heavy atom compounds listed in Table 1 were initially uninterpretable. This problem was overcome, however, by collecting X-ray data sets from crystals soaked in a range of concentrations of gold cyanide starting at 2 mM, where the isomorphous differences between the derivative and native X-ray data sets were 8.9%. At this concentration, a single heavy atom site was identified by visual inspection of the difference Patterson function. This single site allowed protein phases to be calculated that were of sufficient quality that additional sites in the gold cyanide derivative could be located by difference Fourier maps at 4.8 Å resolution. Subsequently, all other heavy atom derivatives were solved by difference Fourier techniques with protein phases derived from the gold cyanide derivative. The positions of the heavy atom sites obtained from these difference Fourier maps were checked against the corresponding difference Patterson maps. Those derivatives that provided useful phase information were recollected to 2.8 Å resolution. This required data collection from multiple crystals. The low- and high-resolution data sets were not

Table 1: Data Collection and Refinement Statistics[a]

data set	concn (mM)	time (days)	resolution (Å)	unique reflections	redundancy	completeness (%)	R_{merge}[b]	R_{iso}[a]	sites	phasing power[d]
native I	–	–	30−4.8	42 182	2.3	97.8	4.6	–	–	–
$KAu(CN)_2$	25	4	30−4.8	38 737	1.9	89.8	4.7	12.9	27	1.16
$KAu(CN)_2$	50	7	30−4.8	41 969	1.8	97.3	7.3	21.2	28	0.82
Me_3PbOAc	50	10	30−4.8	41 055	1.5	95.2	6.7	15.3	17	0.63
K_2PtCl_4	3	1	30−4.8	41 881	2.1	97.1	5.5	19.7	32	0.73
$(NH_3)_2Pt(NO_2)_2$	5	7	30−4.8	41 174	2.0	95.5	6.2	20.2	28	0.80
native II	–	–	30−2.8	206 423	3.4	96.7	7.4	–	–	–
$KAu(CN)_2$	50	5	8.0−3.0	105 448	1.8	63.4	8.1	17.3	23	0.63
$KAu(CN)_2$	50	5	8.0−3.0	120 855	1.9	72.6	8.2	17.4	22	0.59
Me_3PbOAc	50	9	8.0−3.0	116 847	1.7	70.2	8.9	21.2	14	0.37
Me_3PbOAC	50	9	8.0−3.0	50 603	1.2	30.4	9.3	19.8	14	0.45
Me_3PbOAc	50	9	8.0−3.0	69 976	1.3	42.0	7.8	21.8	14	0.44
K_2PtCl_4	3	1	8.0−3.0	120 553	1.8	72.4	7.9	24.8	29	0.41
K_2PtCl_4	3	1	8.0−3.0	94 412	1.7	56.7	7.7	24.2	28	0.44
$(NH_3)_2Pt(NO_2)_2$	5	6	8.0−3.0	131 713	1.9	79.1	8.1	17.9	12	0.46

refinement statistics				rms from ideal values				
resolution (Å)	reflections	total number of atoms	R_{value}[e]	bonds (Å)	bond angles (deg)	torsion angles (deg)	trigonal planes (Å)	other planes (Å)
30−2.8	206 423	44 772	21.5%	0.015	2.24	21.1	0.007	0.012

[a] The data were collected initially to 4.8 Å resolution and subsequently to 2.8 Å. It was not possible to merge the heavy atom data from individual crystals due to slight differences in soaking conditions. Thus, these measurements were treated independently in the heavy atom refinement. The final model, built from the averaged electron density map, was expanded into the tetramer in the crystallographic asymmetric unit, where it was subjected to a final round of least-squares refinement. No adjustments were made to the model in the crystallographic cell. [b] $R_{merge} = \sum(|I_{hi}| - |I_h|)/\sum_{hi}I_{hi} \times 100$, where I_{hi} and I_h are the intensities of individual and mean structure factors, respectively. [c] $R_{iso} = \sum(|F_h| - |F_n|)/\sum_n F_n \times 100$, where F_h and F_n are the heavy atom and native structure factors, respectively. [d] The phasing power is defined as the mean value of the heavy atom structure factor divided by the lack-of-closure error. [e] $R_{value} = \sum(|F_o| - |F_c|)/\sum_n F_o \times 100$, where F_o and F_c are the observed and calculated native structure factors, respectively.

merged because data collected from crystals soaked at different times exhibited significant differences in their degree of substitution.

The heavy atom positions were refined in a cyclical manner to yield a final set of mir phases to 3.0 Å resolution with an overall figure of merit of 0.4. The heavy atom data were placed on the same scale as the native data by a local scaling procedure developed by G. Wesenberg, I. Rayment, and W. R. Rypniewski. Initially, the heavy atom positions and occupancies were refined according to the origin-removed Patterson function correlation method with the program HEAVY (*21*). The resultant protein phases were improved by solvent flattening (*22*) with the algorithm written by W. Kabsch (Heidelberg, FRG). These phases were subsequently employed to find additional minor heavy atom sites and to further refine the positions and occupancies of all of the heavy atom binding sites (*23*).

Examination of the heavy atom positions revealed that many of these sites could be grouped into sets of four which revealed the 222 symmetry of the tetramer. From these sets of heavy atom positions, the locations and orientations of the noncrystallographic 2-fold axes were determined by least-squares refinement. The noncrystallographic symmetry was then applied to the electron density calculated with mir phases. Although the map was noisy, it was possible to manually abstract a molecular envelope that was subsequently employed in cyclical averaging and solvent flattening (*24*). The resulting "averaged" electron density allowed ~1400 residues to be traced readily with few breaks in the connectivity. At this stage, side chains were positioned into the electron density for ~1200 residues with the remainder being left as alanines. This initial model was expanded into the tetramer in the crystallographic cell and refined by the method of least-squares with the program TNT (*25*). An improved set of matrices relating the four molecules in the asymmetric unit was derived from this partially refined model where the exact 222 symmetry of the tetramer was relaxed. This model was also utilized for re-evaluating the molecular envelope. Protein phases, based on this partial model and calculated to 2.8 Å resolution, were combined with the initial mir phases (*26*), and the resulting electron density was subjected to an additional round of solvent flattening, molecular averaging at 2.8 Å resolution, model building, and least-squares refinement. The above procedure was repeated one additional time. The R_{factor} between the calculated structure factors from the final cycle of molecular averaging and the observed data was 17%. Fifty percent of the unit cell volume was included in the final envelope where the expected solvent fraction was 60%.

The final model derived from the averaged electron density described here contains 1446 amino acid residues out of a total of 1455. The small subunit extends from Lys^3 to Thr^{380} with no breaks in the connectivity of the polypeptide chain. The large subunit extends from Pro^2 to Lys^{1073} with only one break between Tyr^{718} and Ala^{724}. In addition to these residues, the current model includes two ADP molecules, three manganese ions, two ornithines, two inorganic phosphates, two potassium ions, one metal of an indeterminate nature, and one water. Overall, the averaged electron density map was exceedingly well-ordered except for several surface loops and, in particular, the region defined by Met^{700}−Val^{750} in the large subunit. A representative portion of the averaged electron density is shown in Figure 1. A Ramachandran plot of the non-glycinyl residues reveals that 87 and 13% of the amino acids adopt dihedral angles lying in the fully and partially allowed regions, respectively, as determined with the program PROCHECK (*27*). The final model, built from the averaged electron density map, was expanded into the tetramer in the crystallographic asymmetric unit where it was subjected to a final round of least-squares refinement (Table

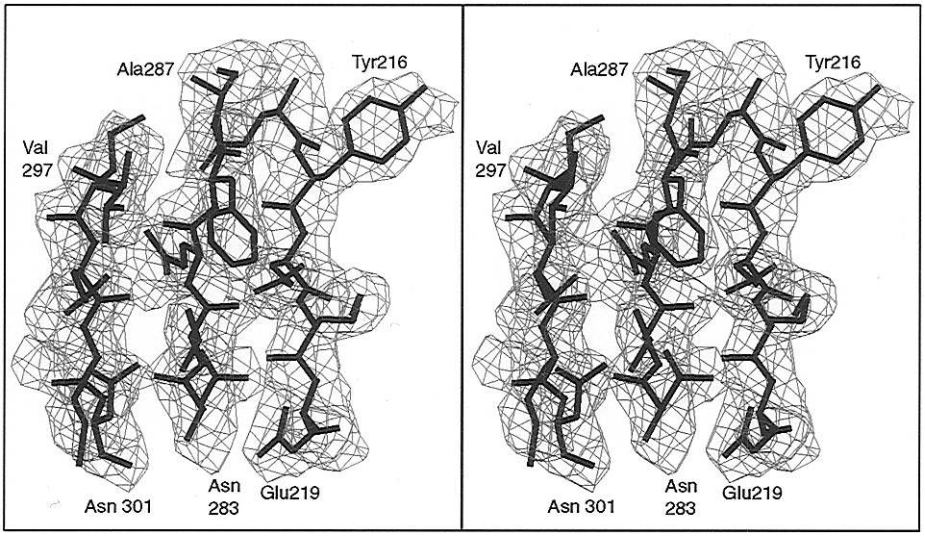

FIGURE 1: Stereoview of a section of representative electron density from the carboxyphosphate synthetic component of the large subunit. The map was cyclically averaged to 2.8 Å resolution starting with "combined" protein phases on the basis of the heavy atom derivatives and the partially refined model using SIGMAA (*26*).

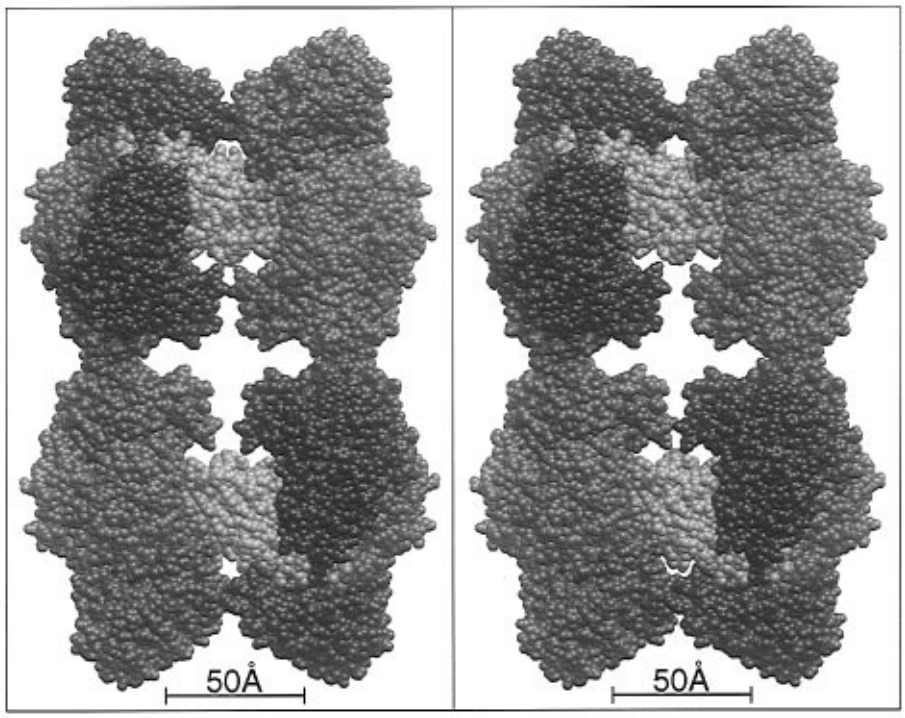

FIGURE 2: Space filling representation of the tetrameric form of CPS. The tetramer was derived by application of the noncrystallographic 222 symmetry to the model for the α,β species built from the symmetry-averaged electron density map. Residues $Met^{1}-Glu^{403}$, $Val^{404}-Ala^{553}$, $Asn^{554}-Asn^{936}$, and $Ser^{937}-Lys^{1073}$ of the large subunit are colored in green, yellow, blue, and red, respectively. These represent the so-called carboxyphosphate, oligomerization, carbamoyl phosphate, and allosteric functional domains of the large subunit. The smaller glutamine amidotransferase subunit is displayed in magenta. The color scheme shown here is maintained throughout the paper. The heterodimers related by the 2-fold rotational axes lying in the plane of the page are shaded differently for distinction. This space filling render of CPS was prepared with the program MOPSY (*58*).

1). The figures shown here were generated from the model built into the averaged electron density.

RESULTS

Quaternary Structure. The structure of CPS described here represents the allosterically activated form of the enzyme due to the presence of ornithine in the crystallization media. Under these conditions, the heterodimeric enzyme oligomerizes to form an $(\alpha\beta)_4$ species (*28, 29*) and exhibits nearly exact 222 molecular symmetry with the rotational relationships between one $\alpha\beta$ species and the other three being 179.9, 178.1, and 178.1°, respectively. As shown in Figure 2, the tetramer is a very large, but open, macromolecular assembly with molecular dimensions of 110 × 200 × 235 Å as measured along the noncrystallographic 2-fold axes. It is characterized by the presence of a substantial irregular hole through the middle of the enzyme with dimensions of 30 × 80 × 35 Å. As might be expected for an assembly that readily interconverts between monomeric and tetrameric states, the interfacial regions between the $\alpha\beta$ species of the tetramer are quite small with protein−protein contacts occurring only along two of the molecular dyads. Specifically, these interactions occur at the interfaces of the allosteric domains that have been identified from biochemical studies

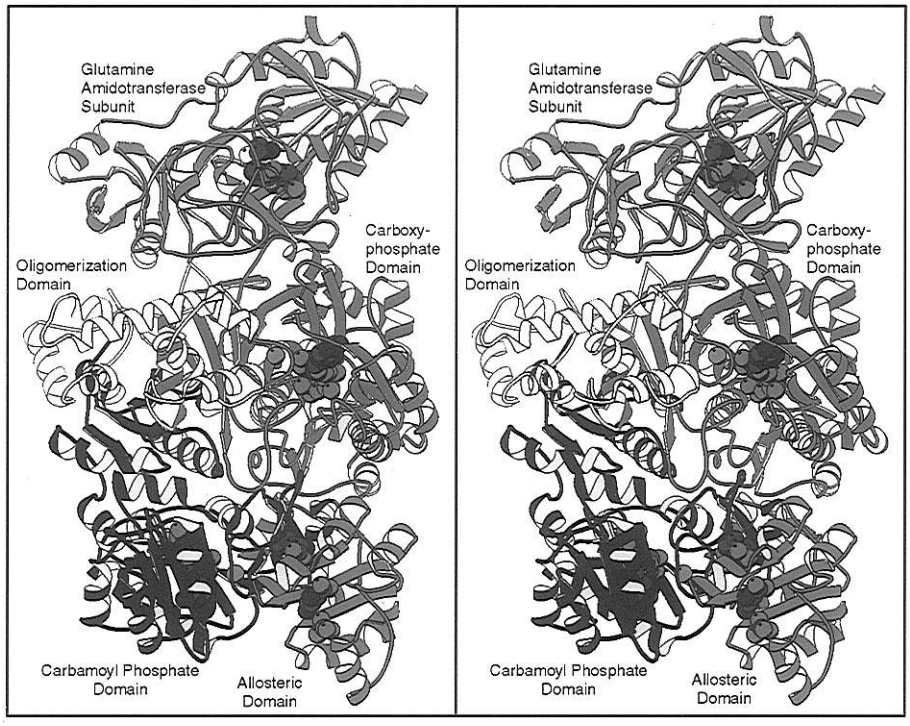

FIGURE 3: Ribbon representation of the large and small subunits. Shown here are the locations of the glutamine binding site, the carboxyphosphate and carbamoyl phosphate active sites, and the allosteric sites. The nucleotides, potassium ions, and ornithines in the large subunit and Cys^{269}, His^{353}, and Glu^{355} in the small subunit are depicted in space filling representations. Figures 3−8 were prepared with MOLSCRIPT (*59*).

(*30*−*33*) and along a portion of the polypeptide chain from Val^{404} to Ala^{553}. These interfaces have buried surface areas of 550 and 575 Å^2, respectively, per $\alpha\beta$ species based on a probe radius of 1.4 Å (*34*). The quaternary structure of the tetramer suggests that the region from Val^{404} to Ala^{553}, for which a biochemical role had not been previously assigned, may function as an oligomerization domain.

The individual heterodimer, as shown in Figure 3, has overall dimensions of 85 × 90 × 105 Å with the large subunit displaying a very uniform shape of approximately equal size in all directions. Asymmetry in the heterodimer is provided by the small subunit that is positioned on one side of the large subunit with essentially no interdigitation of secondary structural elements. This smaller subunit forms its interfacial surface exclusively with the first half of the large subunit in keeping with the chemical need to transfer ammonia derived from the deamidation of glutamine to the carboxyphosphate active site (*12*). In contrast to the tetrameric interface, the buried surface area between the polypeptide chains in the $\alpha\beta$ monomer is extensive with 2100 and 2250 Å^2 contributed by the large and small subunits, respectively.

Structure of the Small Subunit. The small subunit, which contains those amino acids responsible for the glutamine amidotransferase activity of CPS (*8*), displays overall molecular dimensions of approximately 75 × 60 × 60 Å and is distinctly bilobal in shape as can be seen in Figure 4. The NH_2-terminal domain, delineated by Leu^1−Leu^{153}, is composed primarily of four major α-helices and two layers of β-sheet, one of which contains four antiparallel and the other four parallel β-strands. These layers of β-sheet are oriented nearly perpendicular to one another. The COOH-terminal domain is dominated by a ten-stranded mixed β-sheet flanked on either side by two and three α-helices, respectively. This sheet contains five β-strands running parallel. Both the NH_2- and COOH-terminal domains form close associations with the first half of the large subunit of CPS. In addition, the topology of the COOH-terminal domain is exceedingly similar to that observed in GMP synthetase (*35*). Indeed, the rmsd between 129 structurally equivalent α-carbons is 1.7 Å (*36*). The amino acid sequences of the amidotransferase domains of GMP synthetase and CPS demonstrate a 48% similarity and a 27% identity.

From previous biochemical studies, it is known that the active site for the small subunit is located in the COOH-terminal domain. Specifically, Cys^{269} was identified as an essential amino acid in the active site by chemical modification (*37*) and subsequent site-directed mutagenesis experiments (*38, 39*). This residue facilitates the hydrolysis of glutamine by the formation of a glutamyl−thioester intermediate (*40*). Other residues assumed to form part of the active site were identified from amino acid sequence similarities of the small subunit with the class I amidotransferases (*41*). These amidotransferases utilize a conserved Cys-His-Glu catalytic triad to activate the cysteine residue as first identified in the structure of GMP synthetase (*35*). In the small subunit of CPS, these residues, Cys^{269}−His^{353}−Glu^{355}, are located in loop regions near the COOH-terminal portion of the large β-sheet and abut the interface formed by the NH_2- and COOH-terminal halves of the small subunit. The importance of His^{353} has also been confirmed by site-directed mutagenesis (*42*). From the present study, the exact location of the glutamine binding site has not been determined. The replacement of His^{312} with asparagine, however, increases the K_m for glutamine considerably, thus suggesting that this residue is involved in substrate binding (*42*). His^{312} is located in the opposite direction with respect to the catalytic triad approximately 5 Å from Cys^{269}. Interestingly, there is a large opening from the active site to the solvent which could allow ammonia to be released to the solvent. Consequently, it is likely that there are conformational changes associated with the binding of glutamine that serve

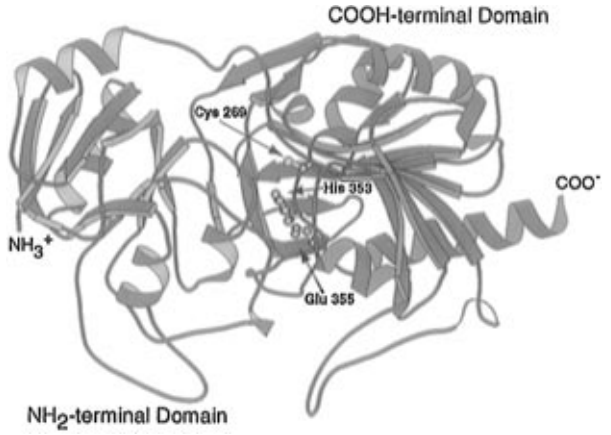

FIGURE 4: Ribbon drawing of the small subunit emphasizing the bilobal domain structure. The catalytic triad of the amidotransferase active site, which abuts the interface between the two domains, is included in ball-and-stick representation.

to prevent the release of ammonia and to maintain catalytic efficiency. Support for such conformational changes within both the large and small subunits is provided by the observed catalytic properties of two site-directed mutants of the small subunit, $Cys^{269}Ser$ and $His^{353}Asn$. These mutant proteins cannot hydrolyze glutamine but can bind the substrate which, interestingly, enhances the rate of ATP hydrolysis within the carboxyphosphate domain by 3.7 (*39*)- and 1.4-fold (*42*), respectively.

Interestingly, both GMP synthetase and the small subunit of CPS are built from two distinct modular domains. In the case of GMP synthetase, the amidotransferase active site is located in the NH_2-terminal domain whereas the COOH-terminal domain catalyzes the amination of xanthosine 5′-monophosphate to form GMP. In both GMP synthetase and the small subunit of CPS, the ammonia released from glutamine is transferred efficiently to a synthetase active site. For GMP synthetase, this active site is located within the same polypeptide chain, whereas for CPS, it is situated on the large subunit. In both cases, the synthetase active sites are separated by a considerable distance from the catalytic cysteine in their respective amidotransferase domains. It has been postulated, in the case of GMP synthetase, that a substantial conformational change is required to couple the enzymatic activities of its two active sites since the structure observed in the crystalline state is rather open and there is an apparent lack of an efficient pathway for the transfer of the ammonia to the synthetase active site (*35*). A large conformational change appears unlikely in CPS, however, on account of the extensive interaction between the entire small subunit and the first half of the large subunit, thereby providing a stable pathway for the transfer of ammonia.

Structure of the Large Subunit. The large subunit has overall dimensions of 88 × 78 × 77 Å and, as expected from amino acid sequence analyses, is folded into two similar halves that are defined by Met^1-Ala^{553} and $Asn^{554}-Lys^{1073}$. A superposition of these halves is shown in Figure 5a. These halves, referred to here as the carboxyphosphate and carbamoyl phosphate synthetic components, share 40% sequence identity for amino acids in the range of Met^1-Glu^{403} and $Asn^{554}-Asn^{936}$ and most likely arose via gene duplication (*9*). In this region, the two halves of the polypeptide chain superimpose with an rmsd of 1.1 Å for 255 equivalent α-carbons and strikingly are related by an almost exact 2-fold rotational axis (179.7°). This dyad symmetry is also observed in the amino acid residues that line the interface between the two halves. Each half contributes 41 residues to the interface, with 21 identical and 14 similar to those in the other half. This represents higher sequence similarity at the interface than that between the two halves as a whole and suggests that CPS arose by gene duplication from an enzyme already existing as an α_2 homodimer.

Both the carboxyphosphate and carbamoyl phosphate synthetic components can be envisioned as consisting of four well-defined domains labeled A−D in Figure 5b. Quite remarkably, the first three domains in each half of the large subunit correspond to those observed in biotin carboxylase, another enzyme that utilizes both ATP and bicarbonate and whose catalytic mechanism is thought to proceed through a carboxyphosphate intermediate (*43, 44*). Other enzymes in this family include D-alanine:D-alanine ligase (*45*), glutathione synthetase (*46*), and succinyl-CoA synthetase (*47*); however, the molecular structure of CPS is most closely related to that observed in biotin carboxylase. Amino acid sequence analyses demonstrate a 47% similarity and a 24% identity between biotin carboxylase and the first half of the CPS large subunit.

The A-domain of the carboxyphosphate synthetic component is defined by Met^1-Gly^{140} and consists of five strands of parallel β-sheet flanked on either side by α-helices. This A-domain superimposes onto that observed in biotin carboxylase with an rms value of 2.0 Å for 89 structurally equivalent α-carbons. Following this modified "Rossmann" fold (*48*), there is a helix−turn−helix motif which leads into the B-domain, as defined in the biotin carboxylase structure (*44*). Like that observed in biotin carboxylase, the B-domain ($Leu^{141}-Leu^{210}$) in the carboxyphosphate half of CPS is defined by a four-stranded antiparallel β-sheet which is covered on the outer surface by two α-helices. The B-domains between CPS and biotin carboxylase correspond with an rms value of 1.7 Å for 44 structurally equivalent α-carbons. The C-domain in CPS is the most complicated of the three motifs and consists primarily of seven strands of antiparallel β-sheet and four major helical regions. This domain superimposes onto that of biotin carboxylase with an rms value of 1.6 Å for 118 structurally equivalent α-carbons. Following the C-domain, the polypeptide chain folds into the fourth or D-domain defined by $Val^{404}-Ala^{553}$. This motif can be envisioned as two globular units, each built from three short α-helices and connected by a longer transitional α-helix. These modules are topologically similar, although the helices differ slightly in length.

In the carbamoyl phosphate synthetic component, the first three domains, delineated by $Asn^{554}-Lys^{686}$, $Leu^{687}-Leu^{756}$, and $Asp^{757}-Asn^{936}$, are nearly identical to those described above for the carboxyphosphate synthetic half. The fourth or allosteric domain ($Ser^{937}-Lys^{1073}$), however, is completely different from the above-described D-domain and consists of five strands of parallel β-sheet and five α-helices forming a Rossmann fold. Interestingly, the topology of this domain is nearly identical to the A-domains of biotin carboxylase and CPS. From biochemical studies, it is known that this region is responsible for the binding of both UMP and ornithine, allosteric effectors of the enzyme (*30*).

Active Sites in the Large Subunit. The active site in the carboxyphosphate synthetic component is located in a pocket formed between the B- and C-domains as displayed in Figure 6a. In the crystal structure described here, this region contains ADP, one inorganic phosphate, and two manganese

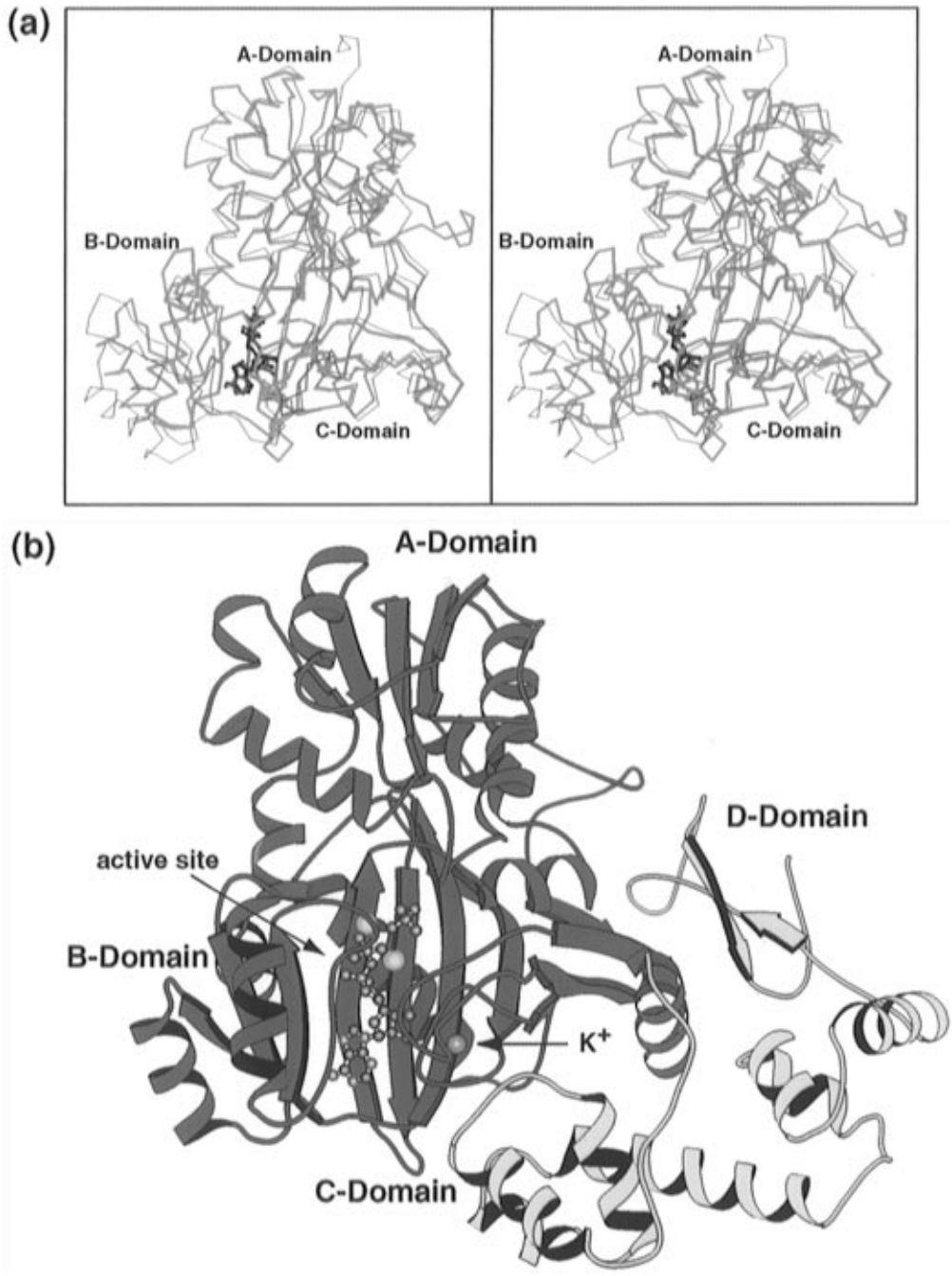

FIGURE 5: Carboxyphosphate synthetic component of the CPS large subunit. Shown in panel a is a superposition of $Met^{1}-Glu^{403}$ (in green) onto $Asn^{554}-Asn^{936}$ (in blue). A ribbon representation of the entire carboxyphosphate domain, from Met^{1} to Ala^{553}, is displayed in panel b. The A-, B-, and C-domains are depicted in green with the sides of the β-strands and the interiors of the α-helices colored in red, blue, and purple, respectively, for the three domains. The D-domain is displayed in yellow.

ions. Due to the resolution of the X-ray data, however, the solvent structure is not clearly defined in the present model. The adenine ring of the ADP abuts the loop region connecting the B- and C-domains. Other than the potential hydrogen bond between the 6-amino group of the adenine ring and the carbonyl oxygen of Glu^{208}, there are few interactions between the purine ring and the protein in this area. The 2′- and 3′-hydroxyl groups of the adenosyl ribose, however, are clearly anchored to the protein via the carboxylate side chain of Glu^{215}. Both Arg^{129}, positioned at the start of the first α-helix in the B-domain, and Arg^{169}, located on a β-strand in the B-domain, interact with the phosphoryl oxygens of the α-phosphate. In addition, the side chain amide group of Gln^{285} lies within hydrogen bonding distance of one of the α-phosphoryl oxygens. This particular residue resides on a β-strand in the C-domain. The phosphoryl oxygens of the β-phosphorus lie within hydrogen bonding distance of the side chain functional groups of Arg^{129} and His^{243}. His^{243} is located in a loop in the C-domain. The inorganic phosphate is surrounded by Arg^{303} and Arg^{306}, both of which are found in the C-domain. One of the manganese ions is coordinated by the side chain of Asn^{301}, a side chain carboxylate oxygen of Glu^{299}, a phosphoryl oxygen donated by the inorganic phosphate, and another phosphoryl oxygen attached to the β-phosphorus of the ADP. The second metal is coordinated via the side chain carboxylate group of Glu^{299}, the same phosphoryl oxygen from the inorganic phosphate, the side chain functional group of Gln^{285}, an α-phosphoryl oxygen from the ADP, and the bridging oxygen between the α- and β-phosphorus atoms of the nucleotide. The coordination surrounding the metals ions, however, is tentatively described at this resolution and will be further

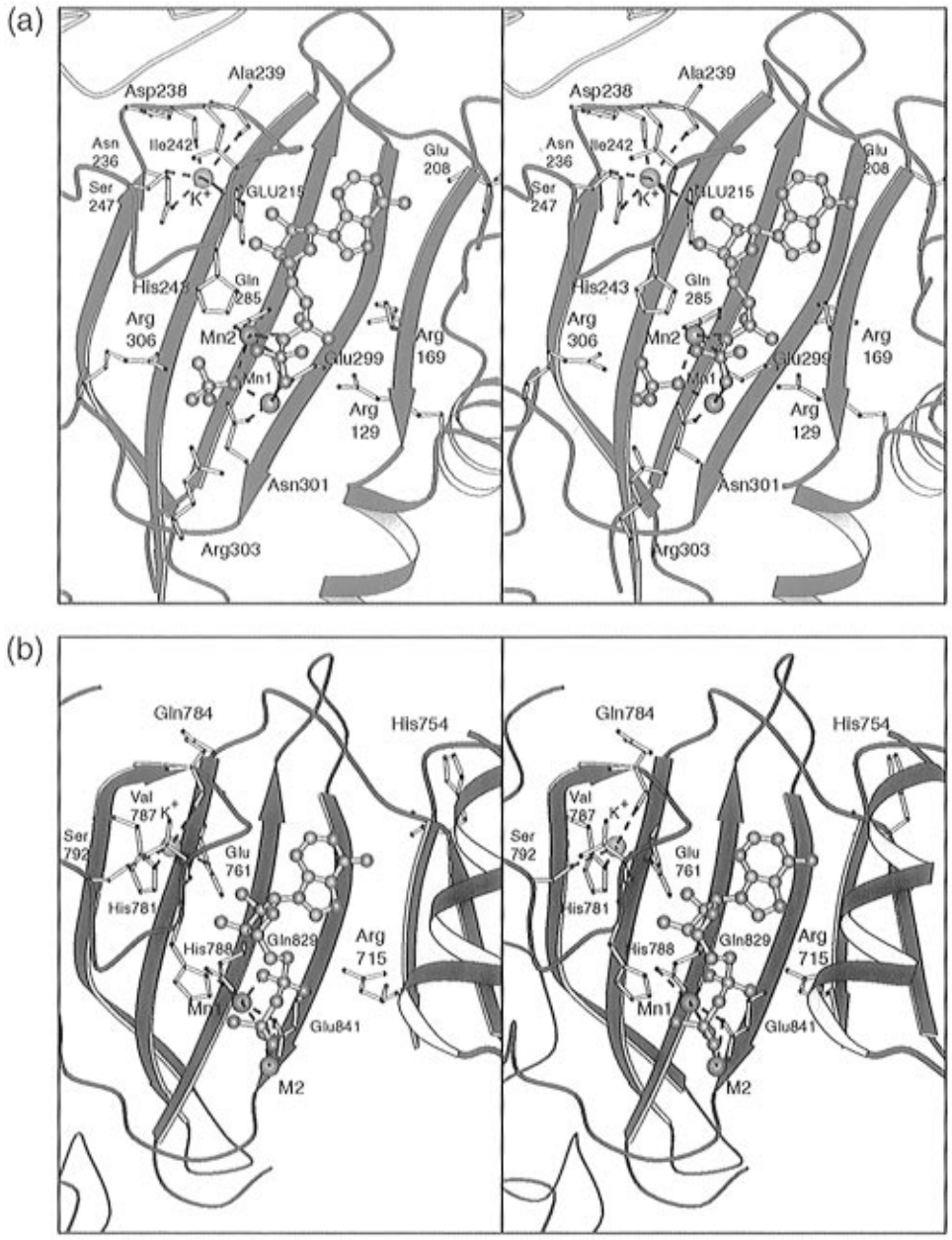

FIGURE 6: Close-up views of the active sites in the large subunit. Shown in panels a and b are the active sites involved in the production of carboxyphosphate and carbamoyl phosphate, respectively. Those side chains within 3.2 Å of the nucleotides and the metals are depicted in ball-and-stick representations.

refined when higher-resolution X-ray data are available. In addition to the two manganese ions, there is a metal ion which is most likely a potassium. This monovalent ion, coordinated by the carbonyl oxygens of Asp[238], Ala[239], and Ile[242] and the side chain oxygens of Glu[215], Asn[236], and Ser[247], is located in a loop in the C-domain and is situated within 4.4 Å of the 2′-hydroxyl group of the adenosyl ribose. The presence of this cation near the active site was anticipated since the activity of CPS has been shown to be potassium-dependent (*49*).

As described above, the three-dimensional motifs of both the carboxyphosphate and carbamoyl phosphate synthetic units of CPS (domains A−C) are similar to those observed in biotin carboxylase, glutathione synthetase, and D-alanine:D-alanine ligase. In the case of the D-alanine:D-alanine ligase model, the X-ray structure was determined in the presence of both ADP and a phosphinophosphate analog (*45*). A comparison between the nucleotide binding sites in the carboxyphosphate synthetic component of CPS and the D-alanine:D-alanine ligase shows that Arg[129], Arg[169], Glu[215], Gln[285], Glu[299], and Asn[301] in CPS are structurally equivalent to Lys[97], Lys[144], Glu[187], Asp[257], Glu[270], and Asn[272] in the ligase. In addition to these specific amino acid residues, the general chemical character of the side chains in contact with the nucleotides is similar in both enzymes.

The active site for the carbamoyl phosphate synthetic component, displayed in Figure 6b, is very similar to that described above for the carboxyphosphate half. In this case, however, the active site contains ADP and two metals but is lacking the inorganic phosphate. Again, the adenine ring abuts the connecting loop between the B- and C-domains, and the 6-amino group of the purine ring lies within hydrogen bonding distance of the carbonyl oxygen of His[754]. The hydroxyl groups of the adenosyl ribose are linked to the protein via Glu[761], while the side chains of Arg[715] and His[788] provide the primary electrostatic interactions between the protein and the α- and β-phosphoryl oxygens of the ADP, respectively. The manganese ion is ligated by an α- and a

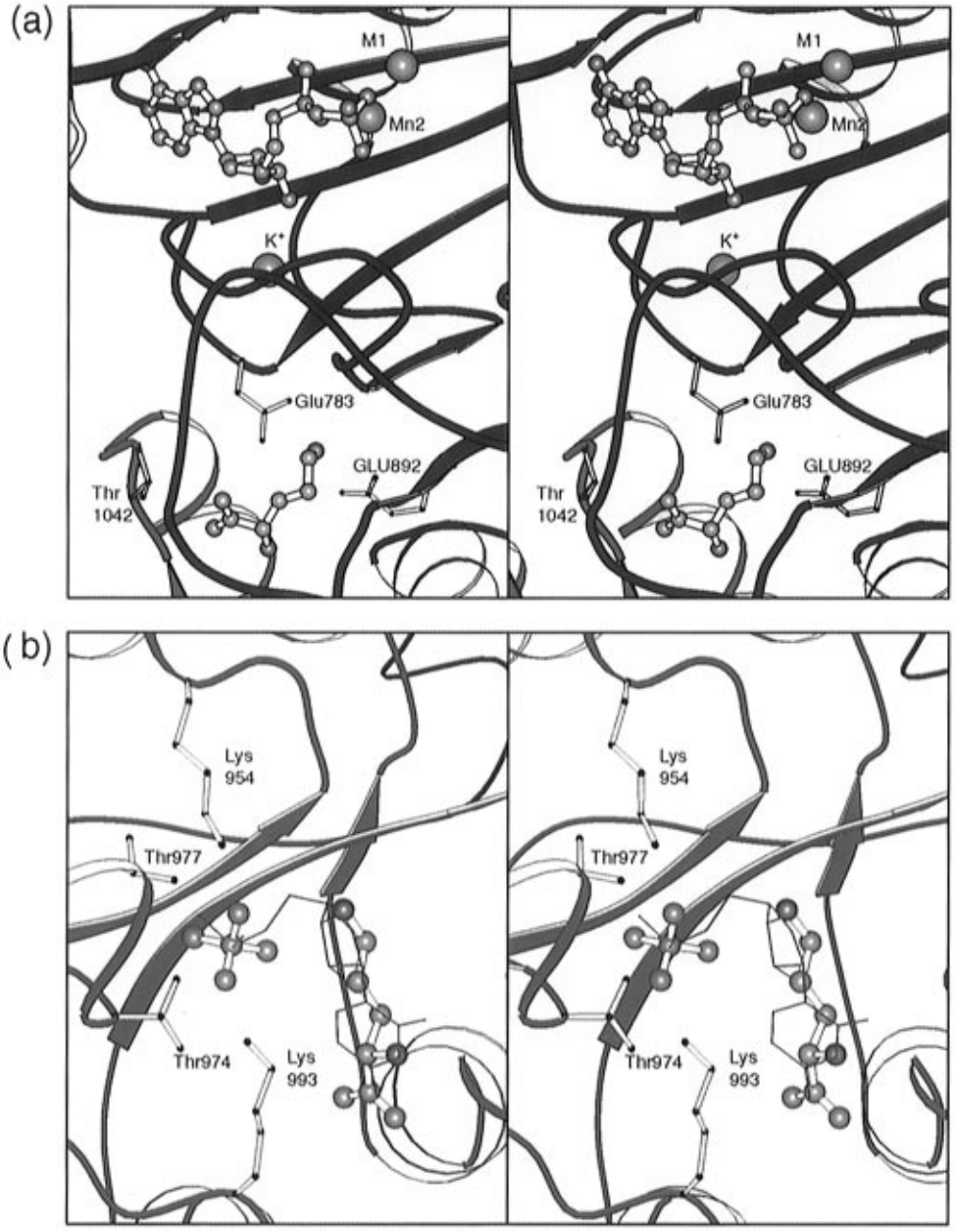

FIGURE 7: Close-up view of the ornithine binding sites in CPS. Shown in panels a and b are the ornithine allosteric site and the putative UMP binding pocket, respectively. Those amino acid residues involved in binding ornithine are depicted in ball-and-stick representations in black and white. In panel b, a skeletal model of UMP is superimposed upon the ornithine and phosphate models.

β-phosphoryl oxygen from the ADP and the side chain groups of Gln^{829} and Glu^{841}. The second metal, of unknown identity, is coordinated by the same β-phosphoryl oxygen and the side chain group of Glu^{841}. Again, there is a putative potassium ion, located in a position nearly identical to that observed in the carboxyphosphate synthetic component, that is surrounded by the side chain groups of Glu^{761}, His^{781}, and Ser^{792} and the carbonyl oxygens of Gln^{784} and Val^{787}. This cation is positioned 4.9 Å from the 2′-hydroxyl group of the adenosyl ribose. Those amino acid residues observed in the carboxyphosphate and carbamoyl active sites described here are in general agreement with past biochemical data (*14, 15*).

As can be seen in Figure 5a, the B-domains associated with the carboxyphosphate and carbamoyl phosphate synthetic components are in slightly different orientations relative to the A- and C-domains. Indeed, because of these arrangements, the carbamoyl phosphate active site, as observed in the structure described here, is more open relative to the carboxyphosphate active site. This is entirely in keeping with the biochemistry in that the carboxyphosphate generated during the reaction must not leave the protein interior while the carbamoyl phosphate so produced must enter the solvent. It also suggests that the B-domains adopt different orientations in the absence of substrates, thereby allowing the binding of nucleotides. The movement of the B-domains is not without precedent as observed in biotin carboxylase (*44*).

Allosteric Sites. Ornithine is known to be an activator of CPS activity (*50*). Two ornithine molecules have been located in the present electron density map, both of which are associated with the allosteric or D-domain of the carbamoyl phosphate synthetic component. The first ornithine binds at a site located at the interface of the C- and D-domains as shown in Figure 7a. Here, the side chain amino group of the activator is hydrogen bonded to the side chain carboxylate group of Glu^{892}. In addition, there is a hydrogen bond formed between the backbone amide nitrogen of Thr^{1042} and the α-carboxyl group of the ornithine.

Presumably, this pocket is the allosteric binding site for ornithine. The second ornithine located in the electron density map is positioned at the COOH-terminal end of the five-stranded parallel β-sheet as displayed in Figure 7b. Here, the side chain amino group of the ornithine is positioned approximately 3 Å from an inorganic phosphate. This inorganic phosphate group interacts with the side chains of Lys^{954}, Thr^{974}, Thr^{977}, and Lys^{993}. Interestingly, site-directed mutagenesis at position 977 abolishes regulation of CPS by UMP while retaining regulation by ornithine (*32*). Additionally, Lys^{993} has been shown to be photolabeled by UMP (*33*). Taken together, these results suggest that the second ornithine and the inorganic phosphate fortuitously bound in the allosteric pocket for UMP and/or IMP.

It is difficult to determine the molecular basis for allostery from a single structure. The mode of inactivation by UMP cannot be explained by the current structure, even though its binding site has been tentatively identified. However, the location of ornithine in the activator site relative to ADP suggests that there is direct coupling between the nucleotide and the effector. Specifically, the side chain amino group and the α-carboxylate of ornithine serve to bridge the C- and D-domains together via Glu^{783} and Glu^{892} and Thr^{1042}, respectively. The carbonyl oxygen of Glu^{783} is situated 3.5 Å from the K^+ which, in turn, lies within 4.5 Å of the adenosyl ribose. Clearly, a three-dimensional model of CPS, solved in the absence of ornithine, will help to more fully define the structural basis of this allostery.

DISCUSSION

The most remarkable feature of the structure of CPS is the distance between the glutamine binding site and the site for the ultimate catalytic step in the synthesis of carbamoyl phosphate. Indeed, S^{γ} of Cys^{269} in the small subunit is 45 Å from the β-phosphorus of the ADP bound in the carboxyphosphate synthetic component, which in turn is 35 Å from the β-phosphorus of the ADP moiety in the carbamoyl phosphate synthetic half. Anderson and Meister (*51*) have demonstrated that, within experimental error, the stoichiometry of the chemical reaction is precisely 2 mol of MgADP and 1 mol of glutamate for every mole of carbamoyl phosphate produced. Thus, there is insignificant uncoupling of the various partial reactions from one another when the concentrations of all substrates are saturating. This fact alone requires that the intermediates of the reaction mechanism, namely, ammonia, carboxyphosphate, and carbamate, must be channeled with nearly 100% efficiency from their site of synthesis to the site of utilization for subsequent chemical events. The shuttling of these intermediates from one site to another must also be mediated directly through the protein matrix in a region that is isolated from the bulk solvent. Since the Michaelis constant for ammonia is 3 orders of magnitude higher than the K_m for glutamine as a nitrogen source (*2*), the ammonia produced from the hydrolysis of glutamine cannot be allowed to come into contact with the exterior solvent. Moreover, the half-life for the decomposition of carbamate at neutral pH is 28 ms (*52*), while the half-life for carboxyphosphate has been estimated to be 70 ms (*53*); thus, each of these intermediates must be protected and stabilized within the protein interior.

The physical coupling of the reactions that must occur within the various functional motifs of CPS must be mediated via conformational changes induced from one domain to another. Support for these conformational changes is derived from the observed enhancement of the rate of glutamine and ATP turnover in the presence of the full complement of substrates (*42*). In addition, the binding of substrates to the large subunit can change the rotational mobility of a nitroxide spin-label attached specifically to the small subunit (*54*). It has been further demonstrated that the chemical reactions catalyzed at each of the active sites can be completely uncoupled from one another. For example, replacement of His^{243} in the large subunit by an asparagine completely prevents the formation of carbamoyl phosphate but does nothing to affect either of the two phosphorylation steps involving MgATP. It has been postulated that this histidine is responsible for the removal of a proton from ammonia during the formation of carbamate from carboxyphosphate (*13*). Mutation of Cys^{248} in the small subunit to an aspartate enhances the rate of the glutaminase reaction 40-fold, but none of the resulting ammonia is retained for the synthesis of carbamoyl phosphate (*16*). The inescapable conclusion from the three-dimensional structure of CPS reported here and the previously determined biochemical properties of the wild-type and mutant proteins is that the ammonia produced at the active site of the small subunit is channeled directly to the large subunit for reaction with carboxyphosphate. The carbamate thus formed must then be channeled directly to the other half of the large subunit for the final phosphorylation by the second MgATP. Incredibly, the nitrogen that originated within glutamine and is ultimately found in carbamoyl phosphate must make a journey of at least 80 Å through the protein interior.

Examination of the structure of CPS immediately suggests a pathway with a contour length of at least 96 Å by which enzymatic intermediates might pass from the active site of the small subunit to the ultimate carbamoyl phosphate active site (Figure 8). This channel was first identified manually and approximated as a series of base points, separated by several angstroms, along its path. The location of the pathway was refined by interpolating between the base points in steps of approximately 0.25 Å while also searching for the location that was farthest from any neighboring protein atom.

Starting at the small subunit, as indicated in Figure 8, there is an opening from the solvent into a substantial cavity lying between the NH_2- and COOH-terminal domains. This cavity, containing the catalytic triad, funnels toward the molecular interface with the carboxyphosphate synthetic component of the large subunit. A channel, delineated on one side by the large β-sheet forming the core of the C-domain and on the other by an α-helix, leads from this interface directly to the carboxyphosphate active site. The average *minimum* radius of the channel between the glutamine and carboxyphosphate active sites is 3.2 Å with a constriction of 2.1 Å which occurs at the side chain of Glu^{217} in the large subunit. It is anticipated that the channel would need a radius of at least 3.2 Å to allow the passage of ammonia. Given the van der Waals radii of the atoms involved, the channel might appear somewhat small; however, given the mobility of the side chains, it is likely that the pathway is large to allow the passage of ammonia from one active site to the other. It is also conceivable that the dimensions of the pathway change during the enzymatic cascade since there is chemical evidence for the activation of the carboxyphosphate active site when the glutamine binding site is occupied (*39, 42*). Interestingly, the entire channel from the glutamine to the

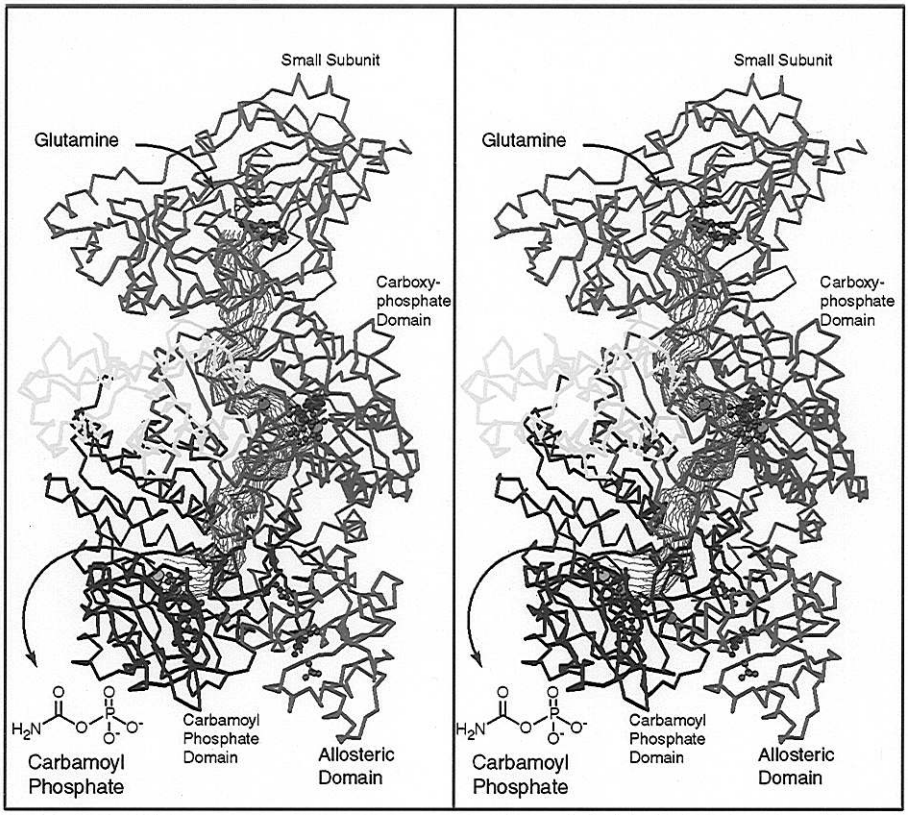

FIGURE 8: Putative channel between the three active sites of CPS. The hypothetical path displayed here was first approximated as a sequence of base points determined by viewing the three-dimensional structure of CPS on an Evans and Sutherland graphics system. A computer program, ALIMENTARY, was subsequently written to refine the positions of these base points and to interpolate a connecting path between them. The path was defined by finding the position at each step which maximized the distance to the closest neighboring atoms in the molecular model of the protein. The radius of the tube was varied to indicate the distance from its center to the closest protein contact. The average radius of the tube was 3.3 Å with the narrowest point occurring near Glu^{217} (large subunit) at 2.1 Å and the widest point near Gly^{293} (small subunit) at 4.3 Å. The distance along the hypothetical path is 96 Å.

carboxyphosphate active site is lined with groups capable of forming hydrogen bonds with contributions predominantly from polar side chains and various backbone atoms. As might be expected for a pathway by which ammonia is transported, there are very few hydrophobic groups associated with this putative channel.

A substantial cavity connects the carboxyphosphate and carbamoyl phosphate active sites and is formed by the juxtaposition of the A-, B-, and C-domains. This pathway has an average minimum radius of 3.5 Å. At its narrowest point, the channel has a radius of 2.5 Å, and this is associated with a carbonyl oxygen of Ile^{20}. However, this amino acid residue resides in a glycine-rich section of the polypeptide chain that may be flexible. Interestingly, this cavity, which passes across the 2-fold rotational axis relating the two functional halves of the large subunit, is lined primarily with backbone atoms together with a few polar and hydrophobic side chains. Except for the immediate entries to the individual active sites, there are very few charged side chains in this tunnel. The absence of such residues is consistent with the need to avoid hydrolysis of carbamate during its travel from the carboxyphosphate to the carbamoyl phosphate active site. It is interesting that the pathway connecting the two synthetase active sites is larger than that observed between the small subunit and carboxyphosphate active site. This may, in fact, reflect the larger sized channel needed for diffusion of the carbamate compared to ammonia.

Substrate channeling has been suggested to account for the efficiency of multienzyme complexes (*55*). To date, tryptophan synthase, which catalyzes the last two steps in tryptophan biosynthesis, presents the most convincing structural and biochemical evidence for such a process. In this enzyme, the two active sites are located on different subunits but are connected by a hydrophobic tunnel approximately 25 Å in length through which indole, the chemical intermediate, diffuses (*56*). As in CPS, the activity of the second active site in the catalytic process is modulated in an allosteric manner by the contents of the first (*57*). For CPS, it is now clear that this enzyme also utilizes substrate channeling to achieve the catalytic efficiency of its remarkable reaction and, indeed, sets a new long-distance record in the process.

ACKNOWLEDGMENT

We thank S. M. Mareya, J. A. Banzon-Kelly, M. F. Harmon, F. Javid-Majd, and R. M. Czerwinski for preparation of the protein used in this investigation and Dr. W. W. Cleland for helpful discussions. The comments of H. H. Rayment are also gratefully acknowledged.

REFERENCES

1. Anderson, P. M., and Meister, A. (1966) *Biochemistry 5*, 3164−3169.
2. Raushel, F. M., Anderson, P. M., and Villafranca, J. J. (1978) *Biochemistry 17*, 5587−5591.
3. Raushel, F. M., and Villafranca, J. J. (1979) *Biochemistry 18*, 3424−3429.
4. Braxton, B. L., Mullins, L. S., Raushel, F. M., and Reinhart, G. D. (1992) *Biochemistry 31*, 2309−2316.
5. Braxton, B. L., Mullins, L. S., Raushel, F. M., and Reinhart, G. D. (1996) *Biochemistry 35*, 11918−11924.

6. Anderson, P. M. (1995) in *Nitrogen Metabolism and Excretion* (Walsh, P. J., and Wright, P., Eds.) pp 33−49, CRC Press, Boca Raton, FL.
7. Matthews, S. L., and Anderson, P. M. (1972) *Biochemistry 11*, 1176−1183.
8. Trotta, P. P., Burt, M. E., Haschemeyer, R. H., and Meister, A. (1971) *Proc. Natl. Acad. Sci. U.S.A. 68*, 2599−2603.
9. Nyunoya, H., and Lusty, C. J. (1983) *Proc. Natl. Acad. Sci. U.S.A. 80*, 4629−4633.
10. Piette, J., Nyunoya, H., Lusty, C. J., Cunin, R., Weyens, G., Crabeel, M., Charlier, D., Glansdorff, N., and Pierard, A. (1984) *Proc. Natl. Acad. Sci. U.S.A. 81*, 4134−4138.
11. Rubino, S. D., Nyunoya, H., and Lusty, C. J. (1986) *J. Biol. Chem. 261*, 11320−11327.
12. Post, L. E., Post, D. J., and Raushel, F. M. (1990) *J. Biol. Chem. 265*, 7742−7747.
13. Miles, B. W., Mareya, S. M., Post, L. E., Post, D. J., Chang, S. H., and Raushel, F. M. (1993) *Biochemistry 32*, 232−240.
14. Javid-Majd, F., Stapleton, M. A., Harmon, M. F., Hanks, B. A., Mullins, L. S., and Raushel, F. M. (1996) *Biochemistry 35*, 14362−14369.
15. Stapleton, M. A., Javid-Majd, F., Harmon, M. F., Hanks, B. A., Grahmann, J. L., Mullins, L. S., and Raushel, F. M. (1996) *Biochemistry 35*, 14352−14361.
16. Mareya, S. M., and Raushel, F. M. (1994) *Biochemistry 33*, 2945−2950.
17. Thoden, J. B., Raushel, F. M., Mareya, S., Tomchick, D., and Rayment, I. (1995) *Acta Crystallogr. D 51*, 827−829.
18. Kabsch, W. (1988) *J. Appl. Crystallogr. 21*, 67−71.
19. Kabsch, W. (1988) *J. Appl. Crystallogr. 21*, 916−924.
20. Wesenberg, G., and Rayment, I. (1997) manuscript in preparation.
21. Terwilliger, T. C., and Eisenberg, D. (1983) *Acta Crystallogr. A 39*, 813−817.
22. Wang, B. C. (1985) in *Methods in Enzymology* (Wickoff, H. W., Hirs, C. H. W., and Timasheff, S. N., Eds.) pp 90−112, Academic Press, San Diego.
23. Rould, M. A., Perona, J. J., Soll, D., and Steitz, T. A. (1989) *Science 246*, 1135−1142.
24. Bricogne, G. (1976) *Acta Crystallogr. A 32*, 832−847.
25. Tronrud, D. E., Ten Eyck, L. F., and Matthews, B. W. (1987) *Acta Crystallogr. A 43*, 489−501.
26. Read, R. J. (1986) *Acta Crystallogr. A 42*, 140−149.
27. Laskowski, R. A., MacArthur, M. W., Moss, D. S., and Thornton, J. M. (1993) *J. Appl. Crystallogr. 26*, 283−291.
28. Powers, S. G., Meister, A., and Haschemeyer, R. H. (1980) *J. Biol. Chem. 255*, 1554−1558.
29. Anderson, P. M. (1986) *Biochemistry 25*, 5576−5582.
30. Rubio, V., Cervera, J., Lusty, C. J., Bendala, E., and Britton, H. G. (1991) *Biochemistry 30*, 1068−1075.
31. Liu, X., Guy, H. I., and Evans, D. R. (1994) *J. Biol. Chem. 269*, 27747−27755.
32. Czerwinski, R. M., Mareya, S. M., and Raushel, F. M. (1995) *Biochemistry 34*, 13920−13927.
33. Cervera, J., Bendala, E., Britton, H. G., Bueso, J., Nassif, Z., Lusty, C. J., and Rubio, V. (1996) *Biochemistry 35*, 7247−7255.
34. Zhang, X.-J., and Matthews, B. W. (1995) *J. Appl. Crystallogr. 28*, 624−630.
35. Tesmer, J. J. G., Klem, T. J., Deras, M. L., Davisson, V. J., and Smith, J. L. (1996) *Nat. Struct. Biol. 3*, 74−86.
36. Rossmann, M. G., and Argos, P. (1975) *J. Biol. Chem. 250*, 7525−7532.
37. Meister, A. (1989) in *Advances in Enzymology and Related Areas of Molecular Biology* (Meister, A., Ed.) Vol. 62, pp 315−374, Wiley, New York.
38. Rubino, S. D., Nyunoya, H., and Lusty, C. J. (1987) *J. Biol. Chem. 262*, 4382−4386.
39. Mullins, L. S., Lusty, C. J., and Raushel, F. M. (1991) *J. Biol. Chem. 266*, 8236−8240.
40. Lusty, C. J. (1992) *FEBS Lett. 314*, 135−138.
41. Zalkin, H. (1993) *Adv. Enzymol. Relat. Areas Mol. Biol. 66*, 203−309.
42. Miran, S. G., Chang, S. H., and Raushel, F. M. (1991) *Biochemistry 30*, 7901−7907.
43. Ogita, T., and Knowles, J. R. (1988) *Biochemistry 27*, 8028−8033.
44. Waldrop, G. L., Rayment, I., and Holden, H. M. (1994) *Biochemistry 33*, 10249−10256.
45. Fan, C., Moews, P. C., Walsh, C. T., and Knox, J. R. (1994) *Science 266*, 439−443.
46. Yamaguchi, H., Kato, H., Hata, Y., Nishioka, T., Kimura, A., Oda, J., and Katsube, Y. (1993) *J. Mol. Biol. 229*, 1083−1100.
47. Wolodko, W. T., Fraser, M. E., James, M. N. G., and Bridger, W. A. (1994) *J. Biol. Chem. 269*, 10883−10890.
48. Rossmann, M. G., Liljas, A., Branden, C.-I., and Banaszak, L. J. (1975) in *The Enzymes* (Boyer, P. D., Ed.) pp 61−101, Academic Press, New York.
49. Anderson, P. M., and Meister, A. (1966) *Biochemistry 5*, 3157−3163.
50. Pierard, A. (1966) *Science 154*, 1572−1573.
51. Anderson, P. M., and Meister, A. (1965) *Biochemistry 4*, 2803−2809.
52. Wang, T. T., Bishop, S. H., and Himoe, A. (1972) *J. Biol. Chem. 247*, 4437−4440.
53. Sauers, C. K., Jencks, W. P., and Groh, S. (1975) *J. Am. Chem. Soc. 97*, 5546.
54. Raushel, F. M., Rawding, C. J., Anderson, P. M., and Villafranca, J. J. (1979) *Biochemistry 18*, 5562−5566.
55. Srere, P. A. (1987) *Annu. Rev. Biochem. 56*, 89−124.
56. Hyde, C. C., Ahmed, S. A., Padlan, E. A., Miles, E. W., and Davies, D. R. (1988) *J. Biol. Chem. 263*, 17857−17871.
57. Pan, P., Woehl, E., and Dunn, M. (1997) *Trends Biochem. Sci. 22*, 22−27.
58. Wesenberg, G. (1997) University of Wisconsin, Madison, WI.
59. Kraulis, P. J. (1991) *J. Appl. Crystallogr. 24*, 946−950.

BI970503Q